PCCP



PAPER View Article Online



Cite this: Phys. Chem. Chem. Phys., 2019, 21, 2992

Effect of surface—bulk partitioning on the heterogeneous oxidation of aqueous saccharide aerosols†

Hanyu Fan, Tadini Wenyika Masaya and Fabien Goulay 🕩 *

The OH-initiated heterogeneous oxidation of mixed saccharide aqueous aerosols is investigated using an atmospheric-pressure flow tube coupled to off-line analysis of the particle composition. For equimolar monosaccharide/disaccharide aqueous aerosol mixtures, the decay of the disaccharide is found to be significantly slower than that of the monosaccharide. Molecular dynamics simulations of the mixed aqueous solutions reveal the formation of a ~ 10 Å disaccharide exclusion layer below the water surface. A simple chemical model is developed to discuss the possible effect of the disaccharide surface partitioning on the heterogeneous kinetics. The observed decays are consistent with a poor spatial overlap of the OH radical at the interface with the disaccharide in the particle bulk. The effect of partitioning on the heterogeneous oxidation of atmospheric organic aerosols is discussed.

Received 31st October 2018, Accepted 16th January 2019

DOI: 10.1039/c8cp06785f

rsc.li/pccp

1 Introduction

Multiphase processes in aerosols are known to affect the chemical composition of the atmosphere, its refractive ability, the process of cloud formation, ^{1,2} and ultimately the climate. ³⁻⁶ Models trying to reproduce and predict the chemical composition of the atmosphere ⁷⁻⁹ are still limited by large uncertainties about chemical reactions occurring in the gas phase and in condensed aerosols. ^{6,10} In particular, there is an urgent need to increase our understanding of reactions occurring at or near the gas–liquid interface. ^{1,11-16}

Heterogeneous chemistry in aerosols is controlled by chemical and physical processes occurring both in the particle bulk and at interfaces.^{3,17} The relative importance of these phenomena is greatly dependent on the physical and chemical properties of the particle.^{14,18–22} The chemical transformation of semi-solid (high viscosity) aerosols is mainly controlled by mass transfers between the bulk of the particle and its surface.^{18,23} As the viscosity of the particle decreases, the diffusion coefficients of the reactants and products increase by several orders of magnitude, and mass transfer phenomena are no longer rate-limiting. Although aerosols with low chemical complexity may be comparable to a one-compartment reactor system,²³ there is increasing evidence that processes occurring at or close to the gas-condensed-phase

Department of Chemistry, West Virginia University, Morgantown, West Virginia 26506, USA. E-mail: Fabien.goulay@mail.wvu.edu

interface may control the chemical transformation. ^{11,12,14,15,24} The effect of these interfacial reactions on aerosol chemical aging depends on the relative concentrations of reactive species close to the particle surface.

For a molecule M_i in aqueous solution, Pegran *et al.*²⁵ express its propensity to migrate from the bulk (B) toward an arbitrary air–water interface Σ as a thermodynamic equilibrium $(M_i)_{\rm B} \rightleftarrows (M_i)_{\Sigma}$, with the corresponding partitioning equilibrium constant $K_{\rm p,i}$:

$$K_{\mathrm{p},i} = \frac{[\mathrm{M}_i]_{\Sigma}}{[\mathrm{M}_i]_{\mathrm{B}}} \tag{1}$$

and partitioning Gibbs free energy

$$\Delta_{\mathbf{p}}G^{\circ} = -RT \ln K_{\mathbf{p},i} \tag{2}$$

where $[M_i]_{\Sigma}$ and $[M_i]_{B}$ are the interface and bulk concentrations, R the ideal gas constant, and T the temperature. The activity coefficients are taken to be unity. Surface-active molecules have a negative value of $\Delta_p G^\circ$ and display higher concentrations at the interface than in the bulk. Non-surface-active molecules have a positive partitioning Gibbs free energy and will predominantly be found in the bulk. A $\Delta_p G^\circ$ value of 2 kcal mol⁻¹ corresponds to a molecular concentration 30 times larger in the bulk than at the interface. Sucrose, a surface-inactive organic molecule, has a $\Delta_p G^\circ$ close to 3 kcal mol⁻¹ corresponding to a bulk concentration that is 2 orders of magnitude larger than at the interface. Molecules with intermediate values of $\Delta_p G^\circ$ will be found both in the bulk and at the interface at different ratios. Pegran et $al.^{25}$ suggested that partitioning of polyols in aqueous solutions is likely due to favored interactions of the carbon chain with the

 $[\]dagger$ Electronic supplementary information (ESI) available: Chemical structure of the saccharides, particle size distribution, and surface weighted mean diameter as a function of OH exposure. See DOI: 10.1039/c8cp06785f

Paper

gaseous phase while the hydroxyl groups favors the bulk water. Conformational entropy and rigidity of the ring may also be taken into account. For salt solutions, molecular dynamics (MD) simulations have been successful in quantitatively reproducing the partitioning behavior at water-air interfaces predicting an exclusion layer up to 5 Å.26

Molecular partitioning at the interface greatly changes the liquid surface tension, therefore affecting the capability of an aerosol to act as a seed for cloud formation. Ruehl et al. used a continuous-flow streamwise thermal chamber to measure the size of water droplets formed on mixed organic-ammonium sulfate particles. In the case of non-surface-active organic molecules, their measurements are consistent with cloud condensation models (k-Köler)²⁷ which consider the organic component dissolved in the particle bulk. For surface-activeorganics which strongly depress the particle surface tension compared to that of water, the particle diameter leading to cloud nucleation is found to be up to 60% larger than those predicted by cloud condensation models. The authors developed a compressed film model in order to explain how surface partitioning can alter the cloud nucleation process. Based on these findings, Bé et al.4 performed a systematic investigation of the surface activity of products of α-pinene and β-caryophyllene ozonolysis. The oxidation products derived from β-caryophyllene are found to exhibit significantly greater ability to depress surface tension than those derived from α -pinene. These results highlight the fact that both (1) initial composition and (2) chemical kinetics of the droplet strongly affect the properties of the particle surface. This impacts uptake of surface water but also the uptake of reactive species found in the atmosphere such as OH, O₃, or NO.

Chemistry at the air-liquid interface is known to differ from that of the bulk due to heterogeneity in species composition and solvent-solute interactions. 1,11,12,15 Prisle et al. 24 used X-ray photoelectron spectroscopy to investigate the acid speciation and surface partitioning of aqueous decanoate salts. They found that the addition of NH4+ cations to the bulk resulted in a pronounced enhancement of the acid formed at the surface, likely resulting from a different acid-base chemistry at the interface. In marine aqueous NaCl aerosols, partitioning of the Cl⁻ anion toward the aerosol surface and their reaction with OH radicals have been shown to explain the observed chemical composition of the surrounding gas phase. 12 More recently, Kumar et al. 11 investigated the reactivity of the atmospherically relevant Criegee intermediate with nitric acid at the air-water interface. Their MD simulations suggested that surface reactions led to the formation of hydroxyethyl hydroperoxide, in stark contrast to nitroxyethyl hydroperoxide, which is formed by direct bulk reaction of the Criegee intermediate with nitric acid.

The OH radical is one of the main oxidizing agents found in the atmosphere.3 Its reactions with liquid and semi-solid aerosols is known to contribute to the decay of important organic compounds in the atmosphere. These heterogeneous reaction schemes are initiated by uptake of gas-phase radicals at the particle surface. 15,23 Several studies have suggested that rapid reactions of OH radicals with concentrated organic constituents may be limited to the outermost layers of particles

 $(\sim 1-2 \text{ nm}).^{14,16,18,28}$ A partitioning of reactants between the bulk phase and the interface is therefore likely to have a significant effect on the chemical evolution of aerosols. Recent mass spectrometry investigations by Huang et al. 15 of the OH oxidation of pinonic acid at the air-water interface determined that the influence of interface chemistry significantly depends on the relative presence of reactants near the surface. These results underscore the need to more extensively characterize interfacial competitive oxidation of aqueous species under a wide variety of conditions.

Saccharide molecules are a major constituent of aqueous atmospheric aerosols.²⁹ In particular, levoglucosan is a main component of aerosols emitted during combustion of biomass. 30,31 Levoglucosan reactions with OH radicals have been studied both in the gas³² and particle phase³³ and contribute significantly to the net loss of organic compound. In addition to their relevance to atmospheric chemistry, saccharide aqueous solutions display a wide range of surface tensions²⁵ and may be used as archetypal systems to determine the effect of partitioning on heterogeneous oxidation mechanisms. In the present study, we have characterized the OH-initiated heterogeneous oxidation of equimolar mixed aqueous aerosols of two non-surfaceactive saccharides: a monosaccharide, β-methyl glucopyranoside (MGP), and a disaccharide, lactose (Table S1, ESI†), using an atmospheric-pressure flow tube at room temperature. The relative concentrations of the aerosol reactants and primary products are monitored by off-line analysis as a function of the time-integrated total concentration of OH radical. We found that the kinetic traces of the monosaccharide and disaccharide reactants are significantly different. To gain more detailed insights into this mechanism, MD simulations were carried out, allowing for prediction of reactant concentration profiles near the air-water interface. Stochastic simulations using a simplified chemical model were also performed to support the interpretation of the data. Our experimental results appear to be consistent with the formation of a ~ 1 nm exclusion layer of disaccharides at the particle surface resulting in a more probable reaction of the monosaccharide with the OH radical. The experimental and modeling studies provide clear evidence that partitioning at the interface will affect the chemical evolution of aqueous organic aerosols.

2 Experimental section

Experiments were performed using an atmospheric pressure aerosol flow tube coupled with a Scanning Mobility Particle Sizer (SMPS), Gas Chromatography-Flame Ionization Detector (GC-FID) and Teflon filter collection. The saccharide particles are generated by nebulizing a 5 mg ml⁻¹ saccharide aqueous solution using a constant output atomizer (TSI, model3076) with a 1.5 L min⁻¹ N₂ flow. The wet aerosol passes through a 3 L Erlenmeyer flask and is mixed with 0.25 L min⁻¹ of wet N_2 , 0.15 L min^{-1} of O_2 (5%), and variable amounts of O_3 . Dry N_2 is added to the total gas flow in order to obtain a total flow of 3 L min⁻¹. The resulting flow is injected into a 45 inch long and

PCCP

ion source are maintained at 275 and 300 °C, respectively. The scan range is set from 50 to 650 Da at 0.2 scan s $^{-1}$. The column temperature is programed to increase from 40 °C to 160 °C at a rate of 30 °C min $^{-1}$, from 160 °C to 170 °C at a rate of 2 °C min $^{-1}$, to 300 °C at a rate of 30 °C min $^{-1}$, followed by an isothermal hold at 300 °C for 2 min. The total running time is 16 min. All the samples are injected in triplicate for the

2 inch I.D., quartz tube. In the absence of drying processes, and under saturated water conditions, the particles are considered to be liquid with saccharide concentrations equal to that of the initially prepared aqueous solutions. The average surfaceweighted diameter of the aerosol is 360 nm. The resident time of the aerosol stream in the flow tube is of the order of 46 s. The OH radicals are generated by photolysis of ozone by three UV lamps (UVP, $\lambda = 254$ nm) in the presence of water vapor. Photodissociation of the aqueous saccharide molecules at this wavelength is expected to be negligible due to their low molar extinction coefficient.34 The amount of OH radicals can be varied either by controlling the concentration of ozone in the flow tube or by the number of UV lamps turned on. Ozone is generated by passing a 1.0 L min⁻¹ O₂ flow through an ozone generator (AC-500G, Ozone Solutions, 0.87 g h⁻¹). The aerosol relative surface-weighted diameter and total mass profiles are displays in Fig. S1(a) and (b) (ESI†) and are found not to change significantly as a function of OH exposure.

The OH exposure (the time averaged OH radical concentration) is quantified via a mixed-phase relative rate method using hexane as the gas-phase reference compound. The initial hexane concentration entering the flow tube is 3 ppmV (ml m⁻³). The decay of the relative hexane concentration is monitored by gas chromatography coupled to a flame ionization detector (FID) (Thermo Scientific Trace GC 2000). The gas is sampled onto a capillary column (phase ZB-5, 30 m \times 0.32 mm I.D. and film thickness of 0.5 μ FT, phenomenex) using a six-port valve. Helium is used as carrier gas at a flow rate of 5.0 mL min⁻¹. The OH exposure \langle OH \rangle -t is obtained from the ratio of the hexane signal with and without the photolysis lamps. $^{36-38}$

After the flow tube, $0.3~L~min^{-1}$ of the reacted flow passes through an ozone denuder and is sent to a SMPS (TSI, model 3936) for particle sizing and concentration measurements. Another $0.05~L~min^{-1}$ of the reacted flow passes through a packed potassium iodide tube to remove O_3 before reaching the GC-FID for hexane concentration measurements. The remaining of the particle flow $2.65~L~min^{-1}$ passes through a PTFE (polytetrafluoroethylene) filter (Millipore FALP, $1.0~\mu m$, diameter 47~mm). The collection is performed for 30 min in order to collect about 1 mg of aerosol.

Following the particle collection, the PTFE filter is sonicated twice for 15 min in a 10 mL mixture of ethanol: distilled water (1:1, v/v) together with 1 mg of internal standard xylose at room temperature. The combined (20 mL) extract aliquots are concentrated by rotary evaporation to about 10 mL. The remaining water solvent is removed by freeze drying with a Freeze Dryer (FreeZone 2.5 Plus, LABCONCO). Silylating reagent (1 mL) (pyridine: sylon BTZ (2:1, v-v)) is added to the freeze-dried residue and allowed to react for 3 hour at room temperature.

The silylated mixtures are analyzed using a Trace 1310 Gas chromatograph interfaced with a Single Quadrupole Mass Spectrometer (GC/MS, Thermo Scientific). A capillary column (TG-SQC, 15 m \times 0.25 mm I.D. and film thickness of 0.25 μm , Thermo Scientific) is used with helium as the carrier gas at a constant flow rate of 1.0 mL min $^{-1}$. The MS transfer line and

3 Computational methods

3.1 Stochastic simulations

quantification analysis.

Stochastic simulations are conducted using the Kinetiscope software. The particles are modeled as a collection of 200 compartments stacked together from the center of the particle to its surface. Each compartment is 100 nm \times 100 nm \times 0.5 nm. In a given compartment, the chemistry is described as follows:

$$MGP + OH \rightarrow Products$$
 (R1)

Lactose
$$+$$
 OH \rightarrow Glucose (R2)

Glucose + OH
$$\rightarrow$$
 Products (R3)

The reaction rate coefficients for the OH reactions are inferred from reactions in bulk aqueous solutions and displayed in Table 1.40,41 The model is non-predictive; model parameters presented in Table 1 are adjusted to reproduce the experimental data. The initial number density of saccharides are 1×10^{16} cm⁻³, 100 times lower than the experimental number density. The lower number density is necessary to reduce the simulation time. In the top compartment, three reactions are added to account for the adsorption of the OH gas radicals on reactive sites. A reactive site is defined as a MGP, lactose, or glucose molecule in the compartment. The adsorption rates are displayed in Table 1 and are one order of magnitude larger than the rates found in previous stochastic simulations to account for the lower number density of reactants. The gas phase number density of the OH radicals is maintained at 1×10^{11} cm⁻³. The simulations are run for 10 s corresponding to an overall OH exposure of $1 \times 10^{12} \text{ cm}^{-3} \text{ s}^{-1}$.

The compartments are connected by diffusion of all reactants and products. In the core of the particle, molecules can diffuse in both directions between compartments. In aqueous solutions saccharide diffusion coefficients are of the order of $1 \times 10^{-6} \text{ cm}^2 \text{ s}^{-1.42}$ Such high diffusion coefficients lead to very long simulations. Houle *et al.*¹⁴ have showed that it is

 ${\bf Table~1} \quad {\bf Reaction~and~diffusion~parameters~used~in~the~stochastic~simulation~of~the~heterogeneous~reaction~of~OH~radicals~with~saccharide~particles~$

	OH reaction rate coefficient (cm ³ s ⁻¹)	Bulk diffusion coefficient (cm ² s ⁻¹)	OH adsorption rate (s ⁻¹)
MGP	5×10^{-12}	6.7×10^{-10}	100
Lactose	4×10^{-12}	4.9×10^{-10}	100
	5×10^{-12}	6.7×10^{-10}	100
Products	_	6.7×10^{-10}	_
OH	_	10×10^{-10}	_

possible to decrease the value of the diffusion coefficients while maintaining a well-mixed system. Simulation tests with gradients of lactose and MGP concentrations show that down to a diffusion coefficient of $1\times 10^{-10}~{\rm cm^2~s^{-1}}$, the reactant concentrations become homogeneous within microseconds. Although the diffusion coefficients in Table 1 are orders of magnitude lower than the experimental ones they still lead to well-mixed particles and therefore do not affect the outcome. In order to simulate the partitioning of lactose at the particle–gas interface, the disaccharide is allowed to diffuse only downward in the first few compartments. The initial concentrations of molecules are unchanged.

3.2 Molecular dynamics

Paper

The starting simulation box contained four methyl β-D-glucopyranoside molecules and four lactose molecules, with 1998 TIP3P water molecules in a cubic box with sides 45 Å long. 43 The concentration of both saccharides in solution is set to 0.111 mol L⁻¹. Three-dimensional coordinates of methyl β -Dglucopyranoside and β-lactose were obtained by converting from SDF structures in PubChem (CID 445238 and 6134, respectively) using Open Babel GUI. The CHARMM c36 force field for carbohydrates was used for the sugar molecules.⁴⁴ The 8 sugar molecules were randomly placed in the box using Packmol. 45 Waters were added using the Solvate plugin in VMD. The system was then minimized for 5000 steps and equilibrated for 5 ns at 298 K. Production MD runs were in the isobaricisothermal (NPT) ensemble at 1 atm and 298 K using a 1 fs timestep using a Langevin barostat and thermostat.46 Nonbonded forces used a cutoff of 10 Å, and electrostatic interactions were modeling using the Particle Mesh Ewald method. 47 After equilibration, the periodic cell was enlarged by 45 Å in the negative and the positive direction along the z axis.⁴⁸ Final dimensions of the system were $45 \times 45 \times 135 \text{ Å}^3$ consisting of a 45 Å thick saccharide solution of water parallel to the (x,y)plane with two air-water interfaces along the z axis. The vacuum can be effectively treated as a gas phase since the concentration of nitrogen and oxygen in the gas phase is negligible at these volumes. Production simulations were run for 110 ns (this timescale is longer than the saccharide diffusion time in water). Four independent systems differing in the initial coordinates of the sugar molecules were run to eliminate starting conformations as a contributing factor to any observed results. The 1-D molecular densities were then computed using the density profiles tool plugin for VMD.⁴⁹

4 Experimental results

For rapidly mixed particles the apparent decay rate of the reactant due to reaction with OH radicals can be expressed following:

$$\frac{[\text{saccharide}]_t}{[\text{saccharide}]_0} = \exp(-k\langle \text{OH} \rangle \cdot t)$$
 (3)

where k (cm³ s⁻¹) is the second-order rate constant for OH oxidation, and [saccharide]₀ and [saccharide]_t the number densities (cm⁻³) of the particle phase reactant before the

reaction and at a given OH exposure $\langle \text{OH} \rangle \cdot t$. Because rate coefficients for heterogeneous processes depend on the particle size, the aerosol reactivity needs to be expressed in terms of the effective uptake coefficient γ_{eff} . It is defined as the fraction of OH–particle collisions yielding a reactive loss of a reactant molecule in the particle phase. The reactive uptake is obtained from the reaction rate coefficient according to eqn (4):

$$\gamma_{\rm eff} = \frac{2kd_{\rm p}\rho_0 N_{\rm A}}{3cM} \tag{4}$$

where ρ_0 , M, and $N_{\rm A}$ are the density of saccharides semisolid particles, the molar mass of saccharides and the Avogadro's number, $d_{\rm p}$ is the mean surface-weighted particle diameter, and c is the mean speed of gas-phase OH. In the following sections the rate coefficients for the OH reactions with lactose or MGP are obtained by fitting the observed decays to eqn (3) over the whole experimental OH exposure range. Uptake coefficients for reactions with a specific saccharide are then calculated based on the SMPS particle size data. The uptake coefficients are used to discuss the relative reactivity of the aerosol under different experimental conditions. The uptake coefficients are not corrected for diffusion of the OH radical in the gas phase.

Fig. 1 displays the relative abundance of the MGP (green dots) and lactose (red triangles) reactants in liquid aerosols as a function of OH exposure. Experimental error bars are 2-standard deviations about the mean value from 3 independent measurements. The solid lines are exponential fits over the experimental OH exposure range returning rate coefficients of $4.7(\pm 1.0) \times 10^{-12}~{\rm cm}^3~{\rm s}^{-1}$ and $3.4(\pm 0.9) \times 10^{-13}~{\rm cm}^3~{\rm s}^{-1}$ for MGP and lactose, respectively. The error bars are 2-standard deviations from the fit.

The good exponential fit of the MGP decay trace suggests that the reaction proceeds under pseudo first order conditions

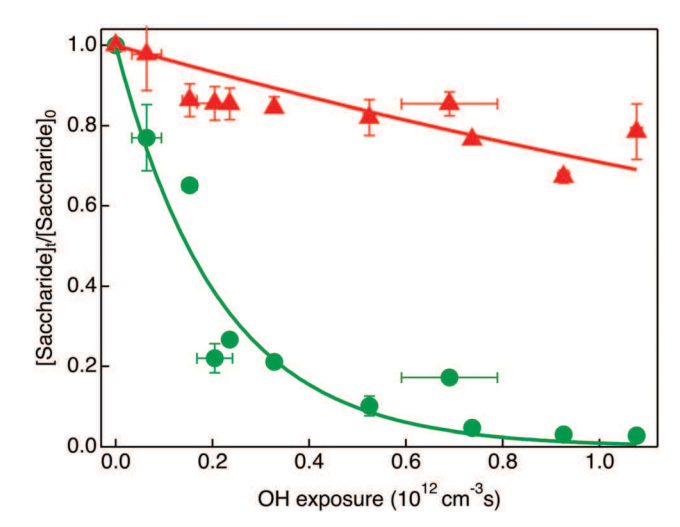


Fig. 1 Relative signal of unreacted methyl β -D-glucopyranoside (green dots) and lactose (red triangles) in mixed equimolar monosaccharide/disaccharide aqueous aerosols as a function of OH exposure. The solid lines are exponential fits to the experimental data over the whole OH exposure range.

PCCP Paper

where diffusion of the reactants is not the rate limiting phenomena. The obtained rate coefficient is higher than the one measured in semi-solid particles below the deliquescence relative humidity (RH) value, ¹⁸ and closed to the bulk value of 5.8×10^{-12} . ³⁹ The uptake coefficient determined using eqn (4) is 5.0 ± 1.1 , suggesting that the reaction proceeds through a complex multistep radical chain mechanism. ³⁶ The rate coefficient obtained from the fitting of the lactose decay, $3.4(\pm 0.9) \times 10^{-13}$ cm ³ s⁻¹, is one order of magnitude lower than that measured in aqueous bulk solution (5.2×10^{-12} cm ³ s⁻¹) ³⁹ and corresponds to an uptake coefficient of 0.4 ± 0.1 . This uptake coefficient is similar to those measured during the oxidation of mixed semi-solid MGP-lactose aerosols at low RH (< 30%). ³⁸

The off-line GC-MS analysis also allows identifying products formed during the heterogeneous oxidation. Fig. 2 displays the relative glucose signal (blue squares) observed during the oxidation of 1:1 MGP-lactose aerosols. The solid line is a fit to the data using eqn (5) corresponding to a pseudo-first order model of the sequential reactions (R4) and (R5):⁵⁰

$$S(\langle \text{OH} \rangle \cdot t) = \left(\frac{S_0 \cdot k_1}{k_2 - k_1}\right) \left(e^{-k_1 \cdot \langle \text{OH} \rangle \cdot t} - e^{-k_2 \cdot \langle \text{OH} \rangle \cdot t}\right)$$
 (5)

Reactant
$$\xrightarrow{OH}$$
 Glucose (R4)

Glucose
$$\xrightarrow{OH}$$
 Products (R5)

where S is the reactant relative signal, k_1 and k_2 are the pseudofirst-order rate constants for the formation and loss of the glucose, and S_0 is proportional to the amount of initial reactants consumed to form the products. In Fig. 2 the formation rate coefficient k_1 is set to that of the MGP decay observed in Fig. 1. The fit to the data returns a rate coefficient k_2 of $9.3(\pm 1.6) \times 10^{-13} \, \mathrm{cm}^3 \, \mathrm{s}^{-1}$ for the glucose oxidation.

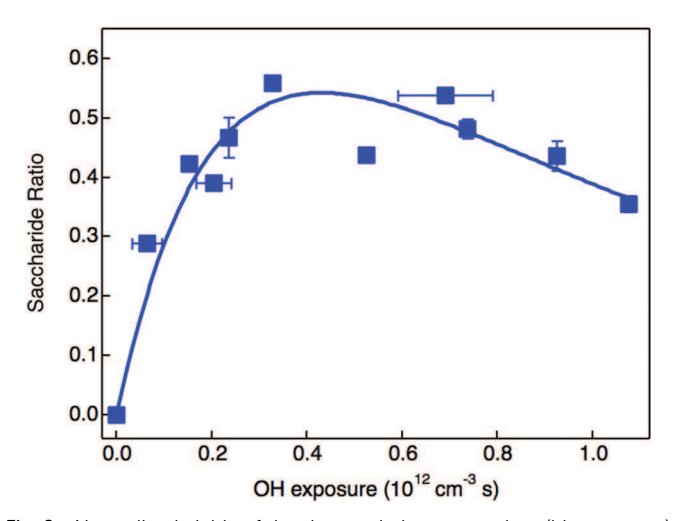


Fig. 2 Normalized yields of the detected glucose product (blue squares) as a function of OH exposure obtained by heterogeneous oxidation of mixed equimolar monosaccharide/disaccharide aqueous aerosols. The solid line is a double experimental fit to the experimental data.

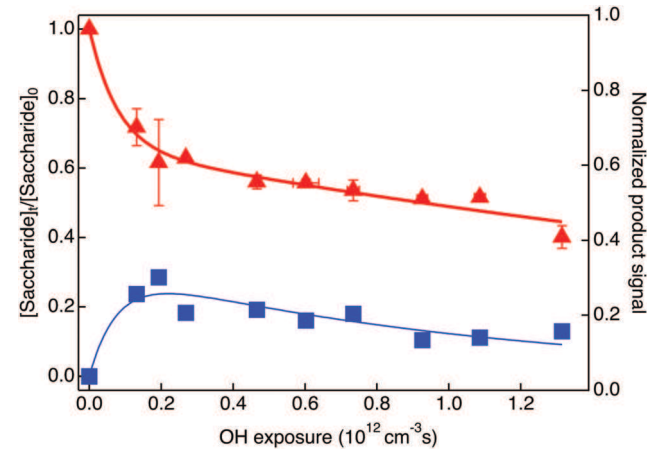


Fig. 3 Relative signal of unreacted lactose (red triangles) and formed glucose (blue squares) in lactose aqueous aerosols as a function of OH exposure. The solid lines are fits to the lactose (thick red line) and glucose (thin blue line) using double exponential functions.

Experiments were also performed with lactose as the sole particle-phase reactant. Fig. 3 displays the relative lactose (red triangles) and glucose products (blue squares) fractions observed during the oxidation of lactose aqueous aerosols. The data are fit with a double exponential function over the experimental OH exposure range. The fit to the lactose profile returns rate coefficients of $13(\pm 5) \times 10^{-12} \text{ cm}^3 \text{ s}^{-1}$ and $3.0(\pm 1.0) \times 10^{-13}$ cm³ s⁻¹. Within the error bars of the fit, the initial fast decay of the lactose reactant is of the same order of magnitude as that observed for the MGP in the mixed particles and corresponds to an uptake coefficient of 10.6 \pm 4.0. The decay rate is found to decrease considerably for OH exposure greater than 2×10^{-13} cm⁻³ s corresponding to an uptake coefficient of 0.4 \pm 0.1. The glucose trace is fit to eqn (5) with k_1 fixed to 13×10^{-12} cm³ s⁻¹, the initial observed lactose decay rate coefficient. The best fit to the data is obtained for a k_2 value of $9.4(\pm 2.0) \times 10^{-13}$ cm³ s⁻¹. This value is similar to that obtained for the decay of glucose in Fig. 2.

5 Simulation outcomes and discussion

Table 2 shows the measured rate coefficients and uptake coefficients for heterogeneous oxidation of saccharide aerosols. It includes previous data on the heterogeneous oxidation of MGP aerosols at RH = 30%, close to the deliquescence point. In bulk aqueous solutions the two saccharides have diffusion coefficients on the order of $1\times 10^{-6}~\rm cm^2~s^{-1},^{40}$ corresponding to diffusion characteristic times of less than 500 μ s (for a 180 nm radius), which is much shorter than the available reaction time. The expected OH-initiated mechanism is fast abstraction of a H-atom from the molecule to from a hydroxy-peroxyl radical. Further reaction with molecular oxygen may lead to peroxy radicals which decompose to give carbonyl molecule and HO₂ radicals. The similar bulk reaction rate coefficients for both saccharides³⁹ suggest similar reactivity toward the OH radical. The different reactive uptake coefficients for

Table 2 Rate constants and uptake coefficients for the heterogeneous oxidation of saccharides aqueous droplet by OH radicals

Molar ratio	Rate constants (cm³ molecule ⁻¹ s ⁻¹)		Uptake coefficients	
(MGP: lactose)	MGP	Lactose	MGP	Lactose
1:0 ^a	$2.0(\pm0.2) \times 10^{-12}$	_	1.9(±0.3)	_
1:1	$2.0(\pm 0.2) imes 10^{-12} \ 4.7(\pm 1.1) imes 10^{-12}$	$3.4(\pm0.9)\times10^{-13}$	$5.0(\pm 1.1)$	$0.4(\pm 0.1)$
$0:1^b$	_ `	$13(\pm 5) \times 10^{-12}$	<u> </u>	$10.6(\pm 4.0)$
	_	$3.0(\pm0.7)\times10^{-13}$	_	$0.4(\pm 0.1)$

^a From Fan et al. ¹⁸ at RH = 30%. ^b Using a biexponential fit function.

the disaccharide and monosaccharide displayed in Table 2 is therefore unlikely to be due to differences in diffusion or reactivity but rather to surface properties. In the following paragraphs we use measured Gibbs free energies²⁵ and molecular dynamics to reveal the extent of partitioning at the interface and discuss its possible effect on the heterogenous kinetics.

Pegran $et~al.^{25}$ used the change of surface tension with concentration at room temperature to infer the partitioning equilibrium constant K_p of polyol aqueous solutions. They found a linear correlation between the calculated solvent accessible surface area (SASA) and the partitioning Gibbs free energy for ethylene glycol, glycerol, glucose and mannitol. In Fig. 4 the Gibbs free energies tabulated by Pagran et~al. are displayed as a function of SASA calculated using Surface Racer $5.^{51}$ The input files are generated using SMILES (simplified molecular input line entry specification)⁵² and the surface areas are calculated with a probe radius of 1.4~Å and tabulated values of van der Waals radii. The SASA obtained using the Surface Racer 5 program appears to be systematically lower than that reported by Pegran $et~al.^{25}$ The red line is a linear fit to the data not including sucrose leading to:

$$\Delta_{\rm p}G^{\circ} ({\rm kcal \ mol}^{-1}) = {\rm SASA} (\mathring{\rm A}^2) \times 0.013 - 3.08$$
 (6)

The systematic shift of the SASA compared to the Pegran et al.25 values does not affect the slope of the fitting function and has only a small effect on the extrapolated values. Pegran et al. excluded sucrose from the fit due to the assumption that the molecule concentration at the interface is null. Extrapolation of the fit (dashed line in Fig. 4) up to 475 Å² returns a sucrose partitioning constant of 0.007, in agreement with the exclusion assumption.²⁵ Fig. 4 also displays the Gibbs free energies for MGP and lactose obtained using calculated SASA values and eqn (6). The obtained $\Delta_p G^{\circ}$ values are 1.04 kcal mol⁻¹ and 3.26 kcal mol⁻¹ for MGP and lactose, respectively. For MGP this corresponds to a concentration at the interface about 6 times lower than that of the bulk. With a $\Delta_{\rm p}G^{\circ}$ value higher than 3 kcal ${\rm mol}^{-1}$, lactose is likely not to be found at the interface creating an exclusion layer close to the surface.

Molecular dynamics simulations are employed to quantify the saccharide partitioning at the interface and estimate the length of the lactose exclusion layer. Fig. 5 displays the averaged normalized atom occurrence profiles obtained from analyzing a 110 ns production run for water (blue dashed line), MGP (green dotted line), and lactose (solid red line) for

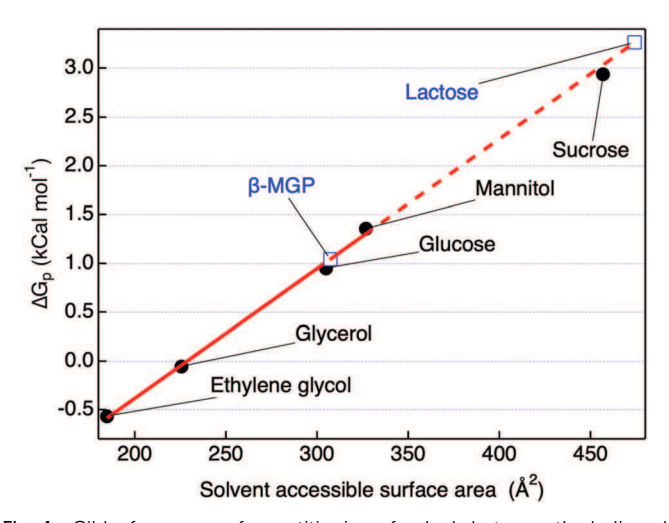


Fig. 4 Gibbs free energy for partitioning of polyols between the bulk and the air—water interface. The accessible solvent accessible surface area are calculated using Surface Racer 5 and the Gibbs free energy values (black dots) are from Pegran *et al.* 25 The solid red line is a linear fit to the data up to mannitol and extrapolated (red dashed line) up to lactose. The blue squares are interpolated and extrapolated Gibbs free energy values for methyl $\beta\text{-}\text{D}\text{-}\text{glucopyranoside}$ and lactose based on their calculated solvent accessible surface area.

4 independent runs, (a) over the entire simulated range and (b) within 15 Å of the water surface. The shading areas are one-standard deviation about the mean from the averaging of 4 independent profiles. The MGP and Lactose profiles are normalized to the area under the curves. The ratio between the areas of the water and saccharide profiles is kept to the water-to-saccharide ratio of the simulations. After 110 ns of simulation, the water molecules diffused outside their initial boundaries. The position of the water surface is determined on both sides of the simulation box by the location at which the water profile derivative reaches 1% of its maximum value. Before averaging, the profiles are shifted to display the water surface on the left at 0 Å.

The lactose profile is found to rapidly decrease close to the surface, generating an exclusion layer with no or very low lactose occurrence of up to 10 Å. Within the first 3 Å of the water surface, the lactose occurrence is found to be up to three orders of magnitude lower than its maximum value in the bulk. In order to quantify the relative saccharide concentration the profiles are integrated within the first 10 Å of the surface. The average ratio for the 8 calculated interfaces between the MGP and lactose integrated profiles is 7 \pm 4. It can also be seen in

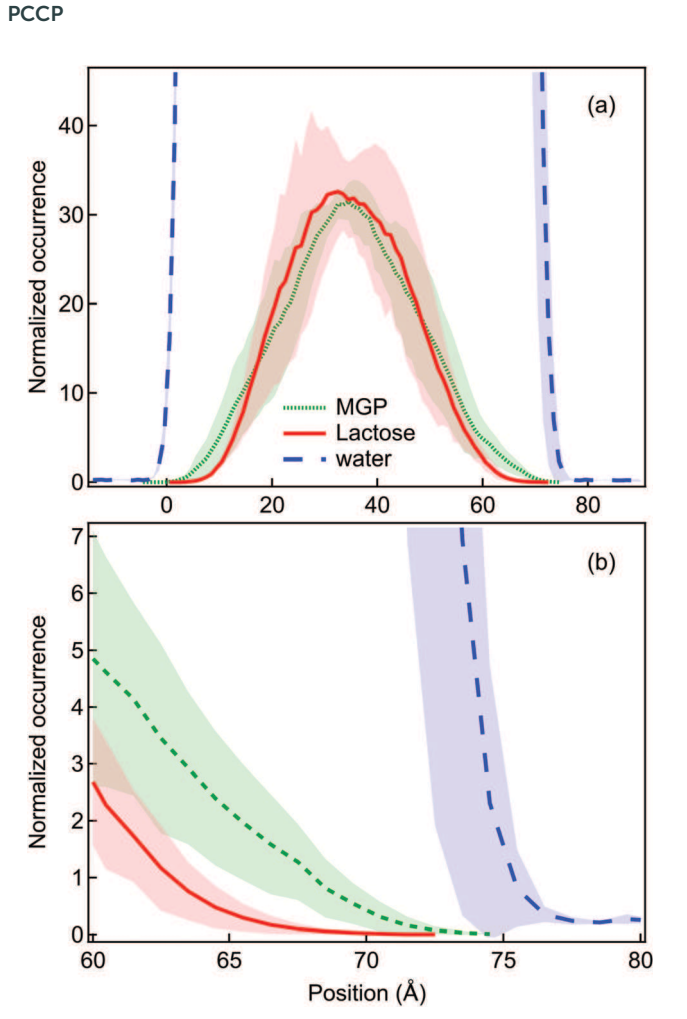


Fig. 5 Simulated average number of atoms occurrence at a given location found after analyzing a 110 ns production simulation run for water (blue dashed line), MGP (green dotted line), and lactose (solid red line) for 4 independent runs (a) over the entire simulated range and (b) within 15 Å of the water surface. The shading areas are one standard deviation about the mean from the 4 independent profiles. The MGP and lactose profiles are normalized by the area under the curve.

Fig. 5(b) that the lactose density is found to be null at the water surface (\sim 73 Å in Fig. 5) while MGP can straddle the air–water interface. Although this probability remains small, it is systematically greater for MGP than for lactose. Fig. 6 shows a snapshot of the simulated open surface for which three MGP molecules are accessible at the water surface for reaction.

The MD simulations together with the thermodynamic information from Pegran $et~al.^{25}$ suggest that the first nanometer of the air–water interface contains mostly monosaccharide and water. The lactose is found only ~ 1 nm or more away from the interface. The size of the lactose exclusion layer may be compared to the reacto-diffusion length, the length an oxidant species can diffuse before reaction. For a 5 mg cm⁻³ saccharide concentration, diffusion coefficient of 1×10^{-6} cm² s⁻¹ and rate coefficient of 5×10^{-6} cm³ s⁻¹ the OH reacto-diffusion length is found to be ~ 1 nm which is comparable to the exclusion layer predicted by the MD simulations. A complete understanding of the effect of surface–bulk partitioning on the OH-initiated oxidation of aqueous

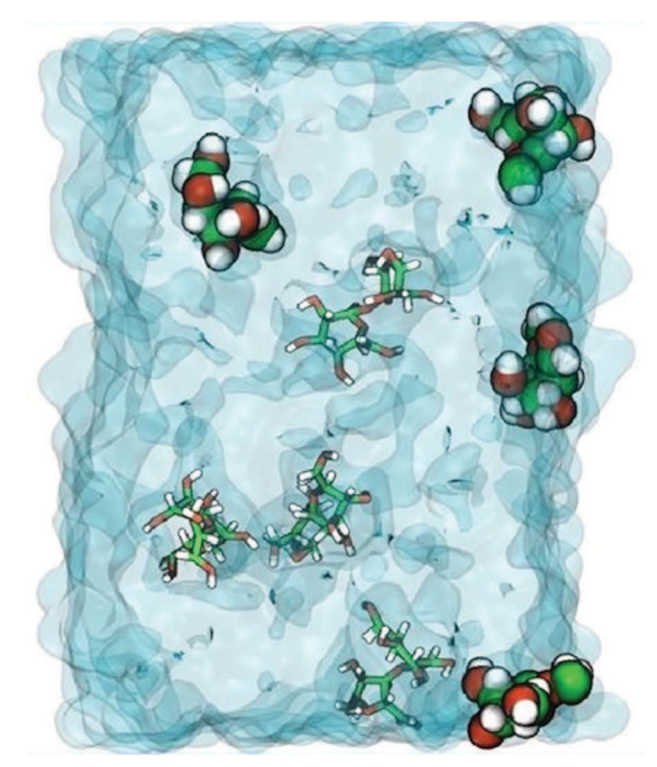


Fig. 6 Snapshot of molecular dynamics simulation showing three of the four MGP molecules at the surface.

aerosols would include intramolecular interactions between the two saccharides, the water solvent, as well as between the reactants and the OH radicals. ¹² Such simulations are outside of the scope of the present study. The stochastic model described below is employed mainly to discuss the possible effect of lactose surface exclusion on the heterogeneous kinetics.

Fig. 7 displays the space integrated MGP and lactose concentrations obtained from stochastic modeling with 1.5 nm (dotted lines), 2 nm (solid lines), and 2.5 nm (dashed lines) lactose exclusion layers. The length of the exclusion layer required to reproduce the experimental trends is only slightly larger than that predicted by the MD simulations. Models performed with no exclusion layer display identical decays for both saccharides. The model returns a fast decay of the monosaccharide as expected for a well-mixed particle with high surface accommodation. The thickness of the lactose exclusion layer has only a minimum effect on the MGP decay profile but strongly affects the lactose decay. Thicker exclusion layers lead to no observable decay of the lactose over the considered OH exposure range.

Fig. 8 shows the time integrated radial profile of the OH concentration (solid red line) for an exclusion length of 2.5 nm (horizontal dashed line). In the model, the lactose is restricted below the dashed line. Because of the fast reaction of the radical with the monosaccharide, there is only a very small amount of OH radicals diffusing below the exclusion layer. For constant adsorption and kinetic rates, as the OH-lactose overlap increases the overall amount of reacting lactose molecules increases, corresponding to an increased decay rate as observed in Fig. 7. The stochastic modeling shows that for

Paper PCCP

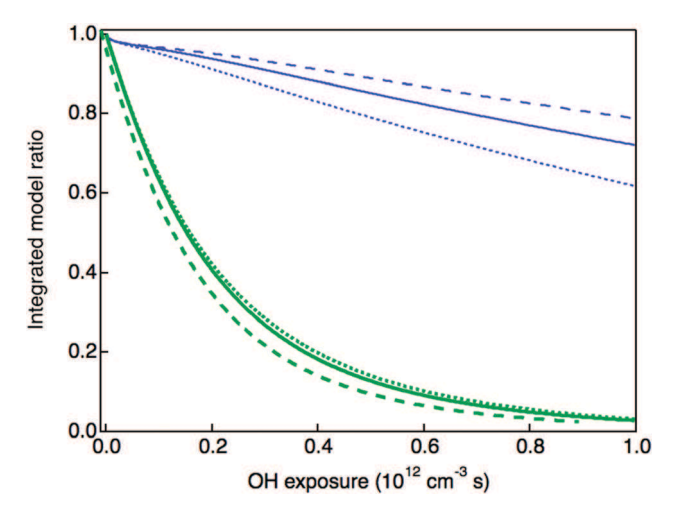


Fig. 7 Modeled MGP (thick green lines) and lactose (thin blue lines) relative decays for surface partitioning of 1.5 nm (dotted lines), 2 nm (solid lines), and 2.5 nm (dashed lines).

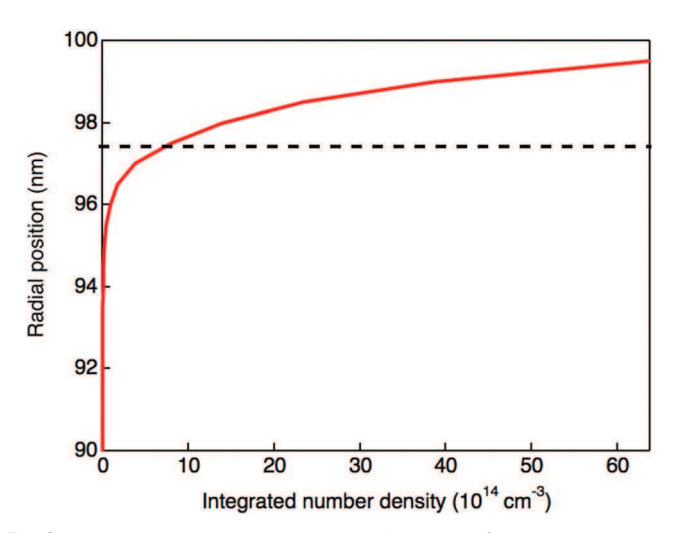


Fig. 8 Time integrated number density of aqueous OH radicals obtained by stochastic simulation of the heterogeneous reaction of OH radicals with equimolar MGP–lactose particles. The dashed line represents the set lower limit of the lactose exclusion layer.

equal MGP and lactose reaction rates and diffusion coefficients, the experimental trends may be reproduce only if there is a sufficient amount of monosaccharide within the disaccharide exclusion layer to react with the OH radicals.

In addition to the effect of the exclusion layer length, the experimental data may also be interpreted based on the probability of finding the saccharide at the open water surface. Knipping *et al.*¹² proposed that the reaction of gaseous OH radicals with Cl⁻ anions at the open water surface is the key step in the formation of gaseous Cl₂ observed in their experiment. A similar interaction of the OH radical with a saccharide exposed at the surface (Fig. 6) would favor reaction with the monosaccharide. In addition, chemical reactions occurring within the few molecular layers of the gas–liquid interface have been shown to proceed with a different mechanisms and/or

different rate coefficient. 11,12,15 Our MD simulations clearly show that the concentration of the monosaccharide will be significantly higher at the interface than that of lactose. If the reaction of the OH radical with saccharide molecules occurs at the interface with a faster rate than in the bulk, partitioning will lead to a large reactivity difference between the two saccharides. As the monosaccharide diffusion to the interface is fast, the reaction decay rate will remain constant as the reaction progresses.

The biexponential decays observed for the oxidation of lactose aqueous aerosols in Fig. 3 may tentatively be explained by involving the formation of glucose as an oxidation product, migrating toward the interface, between the lactose and the surface. Although biexponential behavior may be obtained in the stochastic model by adding higher concentrations of surface active products, the simplified chemical scheme developed here is not sufficient to reproduce the exact observed trends. It is important to notice that the large uptake coefficient observed for the MGP reactant (Table 2) is indicative of complex radical chain reactions where the OH radical is not the sole reactive species in the particle. In aqueous particles, where the diffusion is not a rate limiting step these radicals are likely to be present at the air-water interface as well as in the bulk. The reaction scheme may lead to a wide range of products with different portioning properties. It is possible that some of these products have a higher affinity toward the air-water interface therefore limiting the access of the OH radical to the high lactose concentration in the bulk. Although the experimental and modeling studies presented here do not permit to fully validate these mechanisms, they provide clear evidence that partitioning at the interface will affect the chemical evolution of aqueous organic aerosols.

6 Implications for atmospheric chemistry

Organic aerosols (OA) are introduced in the atmosphere *via* anthropogenic and biogenic sources as well as formed by the chemical reactions and condensation of volatile molecules. They are mostly composed of organic molecules which become more oxidized with aging. The OH radical, being one of the main atmospheric oxidizer, will play an important role in their chemical evolution. The experimental decay rate of the two saccharides measured here combined with the molecular dynamic simulations suggest that partitioning will have a strong effect on the reactivity of aqueous aerosols. For multicomponent well-mixed particles there will be competitive reactions at the surface which will depend on the propensity of the organic molecules to move to the interface. This will be particularly important as the molecular components become more oxidized.

Wan and Yu²⁹ reported the saccharide and polyols composition of atmospheric aerosols collected in urban centers in Hong Kong. Although the composition varies with seasons, levoglucosan, xylose, and fructose appear to be the most abundant saccharides. Non-negligible amounts of the disaccharide trehalose and

PCCP

Table 3 Relative abundance, 29 solvent accessible surface area, and partitioning Gibbs free energy for detected saccharide in atmospheric aerosols. The chemical structures of the saccharide molecules are displayed in Table S1 (ESI)

Saccharide	Relative abundance in aerosols ²⁸	ASA (Ų)	$rac{\Delta_{ m p} G^{\circ}}{({ m kcal} \; { m mol}^{-1})}$
Levoglucosan	1	268.78	0.41
Xylose	0.98	276.39	0.51
Fructose	0.21	311.12	0.97
Trehalose	0.02	445.18	2.71
Melezitose	0.14	635.02	5.18

trisaccharide melezitose are also found during the fall. The chemical structures of the saccharide molecules are displayed in Table S1 (ESI†). Table 3 shows the SASA for the main detected saccharides, the corresponding partitioning Gibbs free energy calculated using eqn (3), and the fall abundance relatively to levoglucosan.²⁹

All the detected saccharides in Table 3 display a positive Gibbs free energy and may be characterized as surface inactive compounds. The extrapolated values of $\Delta_p G^{\circ}$ spam a very broad range corresponding to partitioning constants between 0.5 for levoglucosan and 1.6×10^{-4} for the trisaccharide melezitose. In such mixed particles, levoglucosan will be present at the interface with relatively high concentrations while the trisaccharide will be restricted to the bulk, likely with a large (>1 nm) exclusion layer. Because of the large range of partitioning properties, the interface will display a gradient of concentrations for each saccharide, with the monosaccharide having a higher concentration at the interface than the disaccharide and trisaccharide. The chemical composition of the interface and how it evolves under oxidative conditions will change the optical properties of the particles and their surface tension. This will ultimately affect the reflective property of the atmosphere and the process of cloud nucleation. For multicomponent particles, it becomes vital to understand how the partitioning at the interface will change with the particle aging. Including such effects in atmospheric and cloud formation models may lead to dramatic changes in their predictive abilities. In ternary aqueous aerosols, the interaction of organic molecules with salts such as ammonium sulfate may have an effect on the bulk-interface partitioning and on the overall heterogeneous processes.² Further experimental and modeling studies are necessary to understand how molecular interaction will affect surface processes.

7 Conclusions

The heterogeneous oxidation of mixed saccharide aerosol particles reveals a much higher reactive uptake coefficient for a monosaccharide, β-methyl glucopyranoside than for a disaccharide, lactose. Such a behavior is not expected for molecules in aqueous solutions where the diffusion of the reactants has been shown not to be the rate limiting process. The difference in reactive uptake appears to be consistent with the exclusion of the disaccharide from the surface of the particle, as suggested by earlier empirical

partitioning data.24 Molecular dynamic simulations confirm that in a mixed monosaccharide/disaccharide aqueous solution there is formation of a ~1 nm disaccharide exclusion layer below the particle surface. The disaccharide abundance is low within the first few molecular layers of the air-water interface while that of the monosaccharide is up to one order of magnitude larger. The size of the disaccharide exclusion layer is found to be of the same order of magnitude as the OH reacto-diffusion length.

A simple stochastic model of the system shows that for equal MGP and lactose reaction rates and diffusion coefficients, the experimental trends can be reproduce if there is a sufficient amount of monosaccharide within the disaccharide exclusion layer to react with the OH radicals. The decay of the lactose is found to be strongly dependent on the amount of radicals diffusing below the exclusion layer. The developed model is found insufficient to reproduce the behavior observed for the heterogeneous oxidation of pure lactose aqueous aerosol. In this case, the formation of oxidation products and their diffusion into the exclusion layer may lead to a more complex kinetic behavior.

The study of the heterogenous oxidation of mixed saccharide molecules provides a set of empirical and modeling data to further understand the role of surface-bulk partitioning on atmospheric chemistry. A full understanding of the elementary phenomena controlling the chemical transformation requires systematic investigations of the reactivity of aerosols containing organic compounds with different degrees of oxidation. It is likely that the inclusion of surface partitioning in the chemistry of aqueous aerosols could have a transformative effect on the predictive ability of atmospheric models.

Author contributions

H. F. performed the experiments and the initial data analysis. T. W. M. designed, performed, and analyzed the molecular dynamics simulations.

Conflicts of interest

There are no conflicts to declare.

Acknowledgements

The authors acknowledge the financial support from the WVU Research Corporation through the Program to Stimulate Competitive Research. The authors also thank the West Virginia University High Performance Computing shared facility for providing computing resources and Nicholas Frazee and Blake Mertz for guidance on setting up, running, and analysis of the MD simulations and proofreading the manuscript.

References

1 C. R. Ruehl, J. F. Davies and K. R. Wilson, Science, 2016, 351, 1447-1450.

- 2 H. C. Boyer and C. S. Dutcher, *J. Phys. Chem. A*, 2017, **121**, 4733–4742.
- 3 J. B. Burkholder, J. P. D. Abbate, I. Barnes, J. M. Roberts, M. L. Melamed, M. Ammann, A. K. Bertram, C. D. Cappa, A. G. Carlton and L. J. Carpenter, *et al.*, *Environ. Sci. Technol.*, 2017, 51, 2519–2528.
- 4 A. G. Bé, M. A. Upshur, P. Liu, S. T. Martin, F. M. Geiger and R. J. Thomson, *ACS Cent. Sci.*, 2017, 3, 715–725.
- 5 B. J. Finlayson-Pitts, J. Chem. Soc., Faraday Trans., 2017, 200, 11–58.
- 6 M. Shrivastava, C. D. Cappa, J. W. Fan, A. H. Goldstein, A. B. Guenther, J. L. Jimenez, C. Kuang, A. Laskin, S. T. Martin and N. L. Ng, *et al.*, *Rev. Geophys.*, 2017, 55, 509–559.
- 7 S. R. Utembe, L. A. Watson, D. E. Shallcross and M. E. Jenkin, *Atmos. Environ.*, 2009, 43, 1982–1990.
- 8 L. A. Watson, D. E. Shallcross, S. R. Utembe and M. E. Jenkin, *Atmos. Environ.*, 2008, 42, 7196–7204.
- 9 L. Sheps, B. Rotavera, A. J. Eskola, D. L. Osborn, C. A. Taatjes, K. Au, D. E. Shallcross, M. A. H. Khan and C. J. Percival, *Phys. Chem. Chem. Phys.*, 2017, 19, 21970–21979.
- 10 O. Boucher, D. Randall, P. Artaxo, C. Bretherton, G. Feingold, P. Forster, V.-M. Kerminen, Y. Kondo, H. Liao and U. L'ohmann, Climate Change 2013: The Physical Science Basis; Contribution of Working Group I to the Fifth Assessment Report of the Intergovernmental Panel on Climate, Cambridge University Press, Cambridge, UK, 2013.
- 11 M. Kumar, J. Zhong, X. C. Zeng and J. S. Francisco, J. Am. Chem. Soc., 2018, 140, 4913–4921.
- 12 E. M. Knipping, M. J. Lakin, K. L. Foster, P. Jungwirth, D. J. Tobias, R. B. Gerber, D. Dabdub and B. J. Finlayson-Pitts, *Science*, 2000, 288, 301–306.
- 13 J. Zhong, M. Kumar, J. S. Francisco and X. C. Zeng, *Acc. Chem. Res.*, 2018, **51**, 1229–1237.
- 14 F. A. Houle, A. A. Wiegel and K. R. Wilson, J. Phys. Chem. Lett., 2018, 9, 1053–1057.
- 15 Y. Huang, K. M. Barraza, C. M. Kenseth, R. Zhao, C. Wang, J. L. Beauchanp and J. H. Seinfeld, *J. Phys. Chem. A*, 2018, 122, 6445–6456.
- 16 D. B. Collins and V. H. Grassian, in *Physical Chemistry of Gas-Liquid Interfaces*, ed. J. Faust and J. E. House, Elsevier, 2018, pp. 271–313.
- 17 A. R. Ravishankara, Science, 1997, 276, 1058-1065.
- 18 H. Y. Fan, M. R. Tinsley and F. Goulay, *J. Phys. Chem. A*, 2015, **119**, 11182–11190.
- 19 M. Shiraiwa, A. Zuend, A. K. Bertram and J. H. Seinfeld, Phys. Chem. Chem. Phys., 2013, 15, 11441–11453.
- 20 M. Shiraiwa, M. Ammann, T. Koop and U. Poeschl, *Proc. Natl. Acad. Sci. U. S. A.*, 2011, 108, 11003–11008.
- 21 T. Koop, J. Bookhold, M. Shiraiwa and U. Poeschl, *Phys. Chem. Chem. Phys.*, 2011, **13**, 19238–19255.
- 22 C. Pfrang, M. Shiraiwa and U. Poeschl, *Atmos. Chem. Phys.*, 2011, 11, 7343–7354.
- 23 F. A. Houle, W. D. Hinsberg and K. R. Wilson, *Phys. Chem. Chem. Phys.*, 2015, **17**, 4412–4423.
- 24 N. L. Prisle, N. Ottosson, G. Ohrwall, J. Soderstrom, M. Dal Maso and O. Bjorneholm, *Atmos. Chem. Phys.*, 2012, 12, 12227–12242.

- 25 L. M. Pegram and M. T. Record, J. Phys. Chem. C, 2009, 113, 2171–2174.
- 26 L. M. Pegram and M. T. Record, Chem. Phys. Lett., 2008, 467, 1-8.
- 27 H. Kohler, Trans. Faraday Soc., 1936, 32, 1152-1161.
- 28 A. A. Wiegel, K. R. Wilson, W. D. Hinsberg and F. A. Houle, Phys. Chem. Chem. Phys., 2015, 17, 4398–4411.
- 29 E. C. H. Wan and J. Z. Yu, Environ. Sci. Technol., 2007, 41, 2459–2466.
- 30 G. Engling, C. M. Carrico, S. M. Kreldenweis, J. L. Collett, D. E. Day, W. C. Malm, E. Lincoln, W. M. Hao, Y. Iinuma and H. Herrmann, *Atmos. Environ.*, 2006, **40**, S299–S311.
- 31 G. Engling, J. He, R. Betha and R. Balasubramanian, *Atmos. Chem. Phys.*, 2014, 14, 8043–8054.
- 32 C. Lai, Y. Liu, J. Ma, Q. Ma and H. He, *Atmos. Environ.*, 2014, **91**, 32–39.
- 33 S. H. Kessler, J. D. Smith, D. L. Che, D. R. Worsnop, K. R. Wilson and J. H. Kroll, *Environ. Sci. Technol.*, 2010, 44, 7005–7010.
- 34 M. Kobayashi, H. Utsugi and K. Matsuda, *Agric. Biol. Chem.*, 1986, **50**, 1051–1053.
- 35 J. D. Hearn and G. D. Smith, *Geophys. Res. Lett.*, 2006, 33(L17805), 1–5.
- 36 J. D. Smith, J. H. Kroll, C. D. Cappa, D. L. Che, C. L. Liu, M. Ahmed, S. R. Leone, D. R. Worsnop and K. R. Wilson, *Atmos. Chem. Phys.*, 2009, 9, 3209–3222.
- 37 T. Nah, S. H. Kessler, K. E. Daumit, J. H. Kroll, S. R. Leone and K. R. Wilson, *J. Phys. Chem. A*, 2014, **118**, 4106–4119.
- 38 H. Y. Fan and F. Goulay, in preparation.
- 39 W. D. Hinsberg and F. A. Houle, Kinetiscope, http://www.hinsberg.net/kinetiscope/.
- 40 N. V. Zakatovo, D. P. Minkhadzhiddinova and V. A. Sharpatyi, *Bull. Acad. Sci. USSR, Div. Chem. Sci.*, 1969, **18**, 1520.
- 41 T. Bucknall, H. E. Edwards, K. G. Kemsley, J. S. Moore and G. O. Phillips, *Carbohydr. Res.*, 1978, **62**, 49–59.
- 42 A. C. F. Ribeiro, O. Ortona, S. M. N. Simoes, C. Santos, P. Prazeres, A. J. M. Valente, V. M. M. Lobo and H. D. Burrows, *J. Chem. Eng. Data*, 2006, 51, 1836–1840.
- 43 W. L. Jorgensen, J. Chandrasekhar, J. D. Madura, R. W. Impey and M. L. Klein, *J. Chem. Phys.*, 1983, **79**, 926–935.
- 44 E. R. Hatcher, O. Guvench and A. D. MacKerell, *J. Chem. Theory Comput.*, 2009, 5, 1315–1327.
- 45 L. Martinez, R. Andrade, E. G. Birgin and J. M. Martinez, J. Comput. Chem., 2009, 30, 2157–2164.
- 46 S. E. Feller, Y. H. Zhang, R. W. Pastor and B. R. Brooks, J. Chem. Phys., 1995, 103, 4613–4621.
- 47 U. Essmann, L. Perera, M. L. Berkowitz, T. Darden, H. Lee and L. G. Pedersen, *J. Chem. Phys.*, 1995, **103**, 8577–8593.
- 48 P. Jungwirth and D. J. Tobias, *J. Phys. Chem. B*, 2002, **106**, 6361–6373.
- 49 T. Giorgino, Comput. Phys. Commun., 2014, 185, 317-322.
- 50 J. D. Savee, O. Welz, C. A. Taatjes and D. L. Osborn, *Phys. Chem. Chem. Phys.*, 2012, 14, 10410–10423.
- 51 O. V. Tsodikov, M. T. Record and Y. V. Sergeev, *J. Comput. Chem.*, 2002, 23, 600–609.
- 52 SMILES (simplified molecular input line entry specification), https://cactus.nci.nih.gov/translate/.